PCCP

PAPER

View Article Online
View Journal | View Issue

Cite this: *Phys. Chem. Chem. Phys.*, 2016, **18**, 1998

Symmetry-breaking in the $H_2@C_{60}$ endofullerene revealed by inelastic neutron scattering at low temperature

Salvatore Mamone,*[a] Mark R. Johnson,[b] Jacques Ollivier,[b] Stéphane Rols,[b] Malcolm H. Levitt[c] and Anthony J. Horsewill[a]

Received 20th November 2015,
Accepted 11th December 2015

DOI: 10.1039/c5cp07146a

www.rsc.org/pccp

The fine structure of the rotational ground state of molecular *ortho*-hydrogen confined inside the fullerene cage C_{60} is investigated by inelastic neutron scattering (INS). The INS line corresponding to transitions between the three sub-levels comprising the *ortho* ground state to the non-degenerate *para* ground state was studied as a function of temperature down to 60 mK in neutron energy gain. The experiments show that at ambient pressure the three *ortho* sub-levels are split into a low energy non-degenerate level and a high energy doubly degenerate level separated by 0.135 ± 0.010 meV. This observation is consistent with hydrogen molecules being located at sites with axial symmetry superseding the icosahedral symmetry of isolated rigid C_{60} cages in the solid phase. To gain insight into the role of inter-cage interactions in determining the symmetry breaking potential, the effects of hydrostatic pressure on the fine structure of the line was also investigated. The analysis of the INS spectra shows that the potential and the energy levels of H_2 are sensitive to the orientation of neighbouring cages, consistent with the low-temperature crystalline phase of C_{60}.

1 Introduction

Molecular endohedral fullerenes are supra-molecular complexes in which small molecules are trapped inside fullerene cages.[1] A model example is provided by $H_2@C_{60}$ in which molecular hydrogen, H_2, is permanently entrapped in the nano-cavity of C_{60}.[2] Since its successful synthesis, $H_2@C_{60}$ has been at the centre of intensive theoretical[3–10] and experimental studies, using nuclear magnetic resonance,[11–17] ENDOR spectroscopy,[18,19] infra-red spectroscopy[20–22] and inelastic neutron scattering.[23–26] Molecular hydrogen is a quantum rotor and much of the fascination surrounding such endofullerene complexes pertains to the highly "quantum" nature of the dynamics of the confined molecule. Given its minute confinement, the H_2 molecule exhibits both translational and rotational quantisation on an energy scale in excess of 10 meV.[21,23,24] Indeed, inside its nearly spherical, icosahedral cage, the H_2 molecule possesses translational angular momentum which couples with its rotational angular momentum to produce a manifold of coupled translation–rotation (TR) states.[3–5,27] The degeneracies of these states reveal the symmetry of the confining cage. An icosahedral cage determines highly degenerate TR states, however a lifting of certain degeneracies provides a characteristic signature of any symmetry-breaking in the molecular endofullerene systems.[28] The origin of such lowering in symmetry is of fundamental interest, whether it arises from inter-cage or intra-cage interactions.

Possessing two indistinguishable ^1H nuclei, molecular hydrogen can exist as either one of two nuclear spin isomers, namely *para*-H_2 or *ortho*-H_2, in which the spatial quantum wave-function must be coupled selectively to the nuclear spin wave-function in order to satisfy the Pauli principle. In the ground electronic state only odd rotational angular momentum $J = 1, 3, \ldots$ wave-functions are allowed for *ortho*-hydrogen (nuclear spin $I = 1$) and only even rotational angular momentum $J = 0, 2, \ldots$ wave-functions are allowed for *para*-hydrogen (nuclear spin $I = 0$). In its ground state, *ortho*-H_2 has one quantum of rotational energy and therefore has higher energy than *para*-H_2 in its ground state. The interconversion from one nuclear spin isomer into the other is only possible in the presence of inhomogeneous magnetic fields on a molecular scale, such as those generated by magnetic impurities or dopants. Spin conversion in $H_2@C_{60}$ has been observed in the presence of paramagnetic substances.[13,14,29,30] In the absence of spin-conversion catalysts, *ortho*- and *para*-hydrogen are metastable: no measurable *ortho–para* conversion in solid pure $H_2@C_{60}$ has been observed in experiments that lasted several days at

[a] *School of Physics and Astronomy, University of Nottingham, NG7 2RD Nottingham, UK. E-mail: salvatore.mamone@nottingham.ac.uk, a.horsewill@nottingham.ac.uk*
[b] *Institut Laue-Langevin, BP 156, 38042 Grenoble, France*
[c] *School of Chemistry, University of Southampton, SO17 1BJ Southampton, UK*

cryogenic temperatures.[12,20–23] In both the *para*- and *ortho*-H_2@C_{60} manifold, the energy difference between the ground states and the lowest excited states is in the order of 22 meV, equivalent to 255 K.[21,23,24] Given the typical energy level separations and the *ortho–para* metastability, only the respective rotational ground states, *ortho*-H_2 with $J = 1$, $I = 1$ and *para*-H_2 with $J = 0$, $I = 0$, are effectively populated at any temperature below 50 K. In the following discussion we neglect the nuclear spin degrees of freedom and the nuclear spin structure of the rotational energy levels, except for Pauli exclusion principle effects.

The *ortho*-H_2 ground rotational state consists of three rotational sub-levels with angular momentum $J = 1$. In the gas phase these rotational sub-levels have the same energy. If the icosahedral symmetry of C_{60} is maintained, the three-fold degeneracy should be preserved for hydrogen confined inside the fullerene cage. However the degeneracy of the rotational sub-levels could be lifted in the presence of local perturbations with lower than cubic symmetry. Kohama *et al.* reported an anomaly in the temperature dependence of the specific heat of H_2@C_{60} and interpreted the observation assuming a lifted degeneracy for the $J = 1$ ground state of *ortho*-hydrogen but were unable to identify exactly the type and nature of the symmetry breaking mechanism on a microscopic level.[31] In particular it was not possible to establish to which extent inter-cage interactions are responsible for lowering the symmetry depending on the packing of the molecules in the solid.

In the solid phase the centres of the C_{60} molecules are arranged according to a cubic packing. Solid C_{60} crosses several phase transitions on cooling reflecting variations in the dynamics and structural order of the rotational degrees of freedom.[32] At room temperature the C_{60} molecules rotate almost isotropically[33] and the crystal symmetry is face centred cubic (fcc).[34] Below 255 K, free reorientation is replaced by a ratcheting motion among symmetry equivalent configurations[33] and the low temperature crystal structure of C_{60} is simple cubic ($Pa\bar{3}$) with 4 inequivalent oriented molecules located at one edge and on the centres of the *xy*, *xz* and *yz* faces of the unit cubic cell.[34] In the low temperature phase, the orientation of the C_{60} molecules in the unit cell depends on the detail of the intermolecular potential. The inter-cage interaction potential has two minima with an energy difference of 11.4 meV separated by barrier of 290 meV.[32] These two minima correspond to two possible orientations of neighbouring molecules: in the lowest energy configuration the double bond of one molecule lays opposite to a pentagonal face of a neighbouring molecule (P-orientation) while in the slightly higher energy minimum the double bond of one molecule lays opposite to a hexagonal face (H-orientation), respectively.[35,36] Below 90 K large amplitude molecular re-orientation is inhibited and the proportion of molecules in the two orientations freezes out.[34] At ambient pressure about 85% of the molecules exist in the P-orientation below 90 K while the remainder are in the H-orientation.[37] However if pressure is applied at high temperature and maintained while cooling, the fraction of molecules in the P-orientation is reduced: for example at a pressure of 5 kbar the P-oriented fraction reduces to less than 15%.[37] Interestingly for our study, the site symmetry at the centre of the C_{60} cages is axial ($\bar{3}$) in both orientations with the symmetry axis pointing along principal diagonals of the cubic unit cell.[32]

Here we employ inelastic neutron scattering (INS) to elucidate the effects of symmetry breaking interactions in the quantum dynamics of H_2@C_{60}. INS is able to provide distinctive insight into the energy level structure of H_2 confined in fullerene cages.[23–25,38] Indeed INS has the unique capability to access *ortho–para* transitions in which the total molecular nuclear spin is flipped simultaneously with a change in the rotational state. In this new investigation, the temperature dependence of the INS line corresponding to the transition between the *ortho*-to-*para* $J = 1$ to $J = 0$ states is studied in order to determine the structure of the *ortho*-H_2@C_{60} ground state. By using pressure to change the inter-cage potential in a prescribed manner, we can investigate the origin of the symmetry breaking leading to the lifting of the $J = 1$ rotational degeneracy. The comparative changes in the INS line in experiments with and without pressure provide direct evidence that the lifted degeneracy in H_2@C_{60} is related to inter-cage interactions in the solid phase.

2 Experimental details

H_2@C_{60} was synthesized by the ''molecular surgery'' procedure devised by Komatsu and co-workers.[2] In this way all of the fullerene cages are occupied by a guest molecule. The sample used in the experiments was synthesized by the group lead by Turro from Columbia University (NY).[24,25] In the final stage of the preparation the sample was sublimed to remove occluded solvents and residual impurities. The purified powdered sample with mass 107 mg was thinly wrapped in an aluminium foil sachet for the neutron scattering experiments. Neutron powder diffraction confirmed that the sample was in the cubic phase characteristic of highly pure C_{60} fullerene.

The INS experiments were conducted on the IN5b time-of-flight (TOF) spectrometer at the Institut Laue-Langevin (ILL) in Grenoble, France.[39] All the spectra were recorded at 8 Å for the incident neutron wavelength. In the chosen set-up the instrumental resolution, described by a Gaussian profile, was 0.3 meV (full width at half maximum) in the neutron energy gain region around −14.5 meV, where the H_2@C_{60} transition of interest is located. The temperature dependence of the INS line corresponding to the transitions from the ground *ortho*-H_2 state to the *para*-H_2 ground state (neutron energy gain) was studied first without and then with an applied pressure of 5 kbar. For the experiments conducted at ambient pressure, the sample was mounted inside a ^{3}He/^{4}He dilution refrigerator inserted into a standard ILL 'orange cryostat'. Stable sample temperatures in the range 60 mK $\leq T \leq$ 35 K were achieved. In the experiments with applied pressure, the sample was subjected to hydrostatic pressure up to 5 kbar using ^{4}He as the medium. The pressure cell was mounted directly inside the 'orange cryostat' providing a base temperature of 3.3 K for the

pressure experiments. The data recorded in this investigation is openly available.[40]

3 Results

3.1 Experiments at ambient pressure

The temperature dependence of the inelastic line corresponding to transitions from the *ortho*-H_2 ground state to the *para*-H_2 ground state (neutron energy gain) is shown in Fig. 1. In total 20 datasets were recorded between 35 K and 60 mK at approximately equal steps in the logarithm of temperature, but for clarity only a selection is shown in the figure. Although no structure is fully resolved, the line gets broader and asymmetric, with its centre shifting towards the left (higher neutron energy gain) when the temperature is increased.

The change in line-shape, line-width and peak position, with temperature is inconsistent with transitions from a three-fold degenerate level. A multi-component analysis of the temperature dependence of the line was attempted by assuming an axially-symmetric perturbation, so that the $J = 1$ *ortho* ground state is split into one non-degenerate level and one doubly-degenerate level. Panel (a) of Fig. 2 shows the best fit of the experimental line-shapes to a two-component Gaussian model:

$$N(E;T) = \frac{1}{1+2\exp[-\Delta/k_B T]}\frac{\bar{N}}{\sqrt{2\pi}\sigma}\exp\left[-\frac{(E-\bar{E})^2}{2\sigma^2}\right] + \frac{2\exp[-\Delta/k_B T]}{1+2\exp[-\Delta/k_B T]}\frac{\bar{N}}{\sqrt{2\pi}\sigma}\exp\left[-\frac{(E-\bar{E}+\Delta)^2}{2\sigma^2}\right] \quad (1)$$

where $\bar{E}$ is (minus) the energy of the non degenerate energy level with respect to the *para* ground state, Δ is the energy separation between the non-degenerate and the doubly degenerate *ortho*-levels, $\bar{N}$ is the total number of counts and σ is related to the full width at half maximum of each component $w = 2\sqrt{2\log(2)}\sigma$. In this model the relative intensity of the two components is constrained only by Δ and by the degeneracy of the levels. The experimental data sets were fitted simultaneously for all the recorded temperatures by using $\bar{E}$, Δ, $\bar{N}$ and w as fitting parameters. A linear correction of the background was performed at each temperature before fitting the lines in order to reduce the effects of small systematic errors. The fits reveal a crossover in the

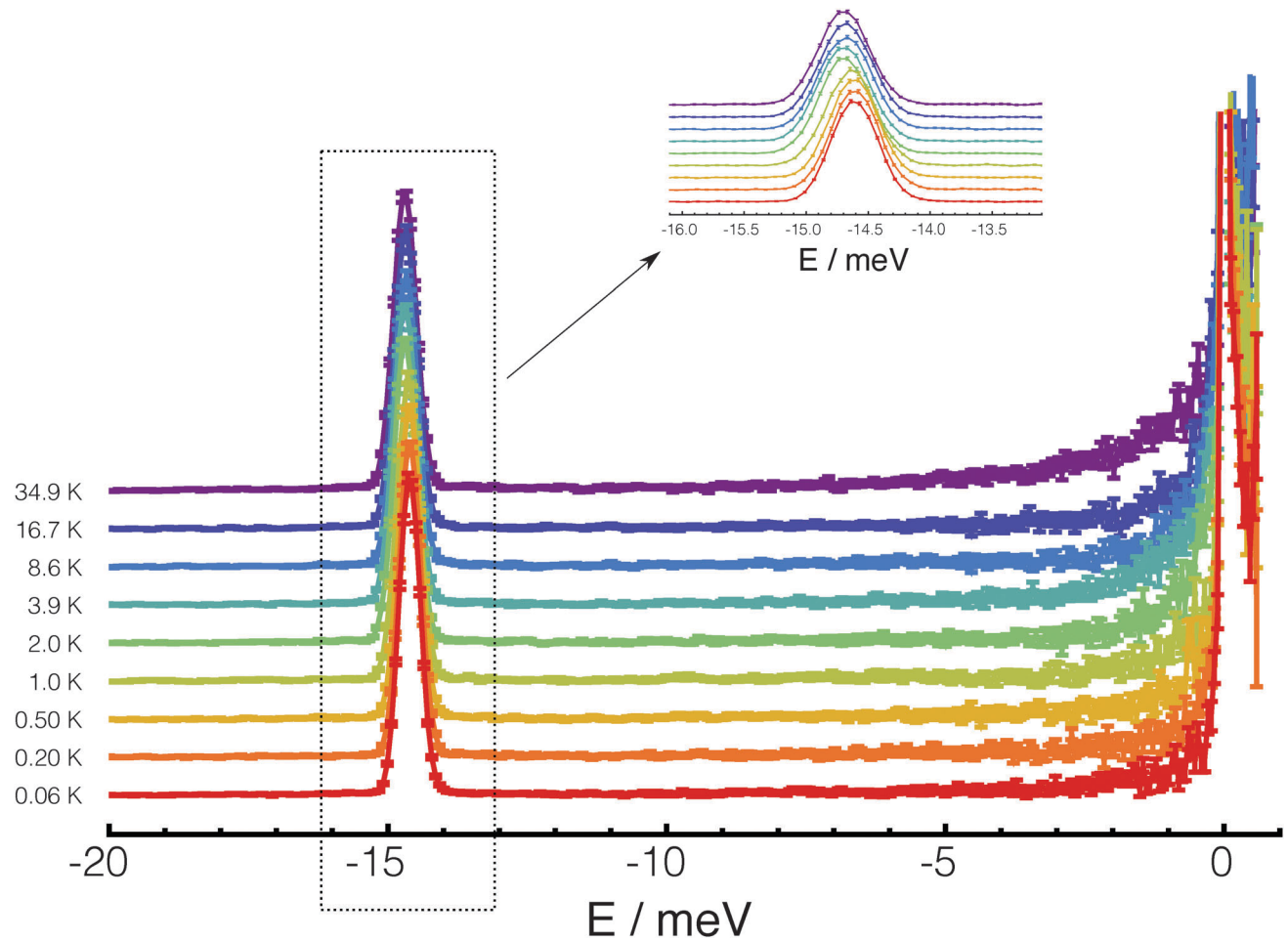

Fig. 1 Low temperature INS spectra of $H_2@C_{60}$ at 8 Å in neutron energy gain. The dashed box encloses the region containing the peak from the *ortho* to the *para* ground state and is zoomed in the inset for clarity.

relative intensities of the two components with increasing temperature. The observations can only be explained with a model in which the low-energy state is non-degenerate and the high-energy state is two-fold degenerate. The best fit values are $\bar{N} = 19.8 \pm 0.2$ for the transition counts, $\bar{E} = -14.60 \pm 0.01$ meV for the centre of the low-energy line, $\Delta = 0.135 \pm 0.01$ meV for the energy separation between the low-energy non-degenerate state and the double degenerate state and $w = 0.45 \pm 0.01$ meV for the full width at half maximum. The corresponding structure of the rotational ground states of $H_2@C_{60}$ is shown in panel (b) of Fig. 2.

The total number of scattered neutrons integrated over the experimental line remains constant with temperature within error bars. The constancy of the counts $\bar{N}$ indicates that: (a) any spin conversion effect is negligible in the time scale of the experiment (3 days), (b) at all the temperatures of interest for this study (less than 40 K) no other *ortho* state is appreciably populated but the ground state and (c) there is no dependence of the transition probabilities on the *ortho* initial state, as discussed below.

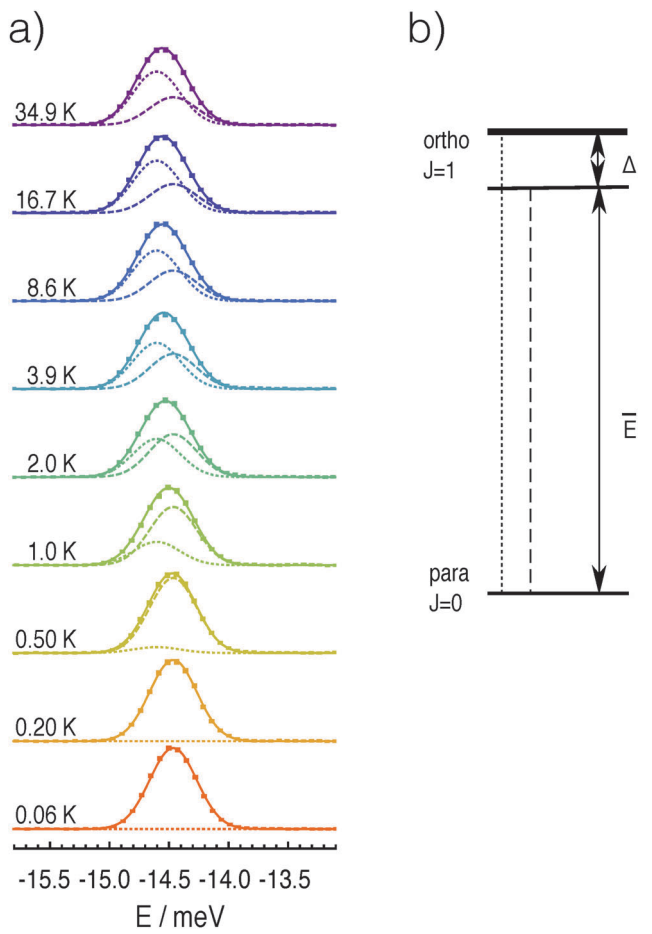

Fig. 2 (a) Experimental INS spectra of the ground state transitions of $H_2@C_{60}$ at various temperatures with error bars (points) and best fit with the two Gaussian model of eqn (1) (lines). The best fit curve is shown as full line for each temperature, while the two components are shown as dashed and dotted lines, respectively. For clarity only data at few selected temperatures are shown. (b) The structure of the two lowest rotational state of $H_2@C_{60}$ as determined from the analysis of the INS experiments.

3.2 Experiments in the pressure cell

To gain insight into the influence of inter-cage interactions, hydrostatic pressure was applied to the sample. The application of pressure affects the sample in two ways: (a) it changes the lattice constant and consequently the distance between cages, which influences the inter-cage interaction potential and (b) it modifies the statistical weights of the P-oriented and H-oriented fullerenes.

In the first set of pressure experiments hydrostatic pressure at 5 kbar was applied to the sample starting from 140 K. The sample was kept under pressure at 5 kbar and cooled down to be studied between 20 K and 3 K. The analysis of the neutron powder diffraction data, recorded simultaneously with the INS spectra, implied a volumetric compression of the unit cell of the order of 5%. In such experimental conditions the fraction of H-oriented *versus* the P-oriented molecules was increased to about 85%[37] allowing a study of the *ortho–para* INS line in the H-rich phase at 5 kbar. In a second set of experiments the temperature was raised to 50 K, the pressure was released, the sample was cooled down and the line was studied again between 20 K and 3 K. In this last set of experiments, contrary to the experiments conducted entirely at ambient pressure, most of the fullerenes are expected to remain locked into the H-orientation with minimal influence on the unit cell parameters.

The low temperature INS spectra of $H_2@C_{60}$ kept under pressure at 5 kbar (applied from 140 K) and after releasing the pressure are shown in panel (a) and (b) of Fig. 3, respectively. Since all the materials that encase the sample (aluminium foil, pressure cell, cryostat) are in the ground state at the temperatures of the study, no peaks other than the $J = 1$ to $J = 0$ transition of $H_2@C_{60}$ are visible in this region of neutron energy gain and 'empty cell' subtraction was not needed in the data analysis.

The best fit of each set of lines with the two component model of eqn (1) is shown in Fig. 3.

3.3 Discussion

The best fit values for the two-Gaussian model parameters are reported in Table 1 for each of the three set of experiments. Although the variation in the position of the centre of the lower energy component $\bar{E}$ is not significant because of experimental uncertainties, a clear trend in the splitting of the *ortho*-$H_2@C_{60}$ ground state can be observed across the three different sets of experiments. The splitting Δ gets larger going from the P-rich phase to the H-rich phase and again to the H-rich phase with applied pressure: the maximum variation in Δ is about 40% between the P-rich phase and the H-rich phase under pressure. These observations indicate that the relative orientation and the distance between cages play a significant role in lifting the degeneracy of the *ortho*-$H_2@C_{60}$ ground state. This is also seen by plotting the temperature dependence of the first moments of the best-fit model to the rotational INS peak, see Fig. 4. The range of variation and the turning point of the curves describing the temperature dependence of the first moments are determined by Δ, since Δ influences both the Boltzmann factor determining the relative weight of the two components

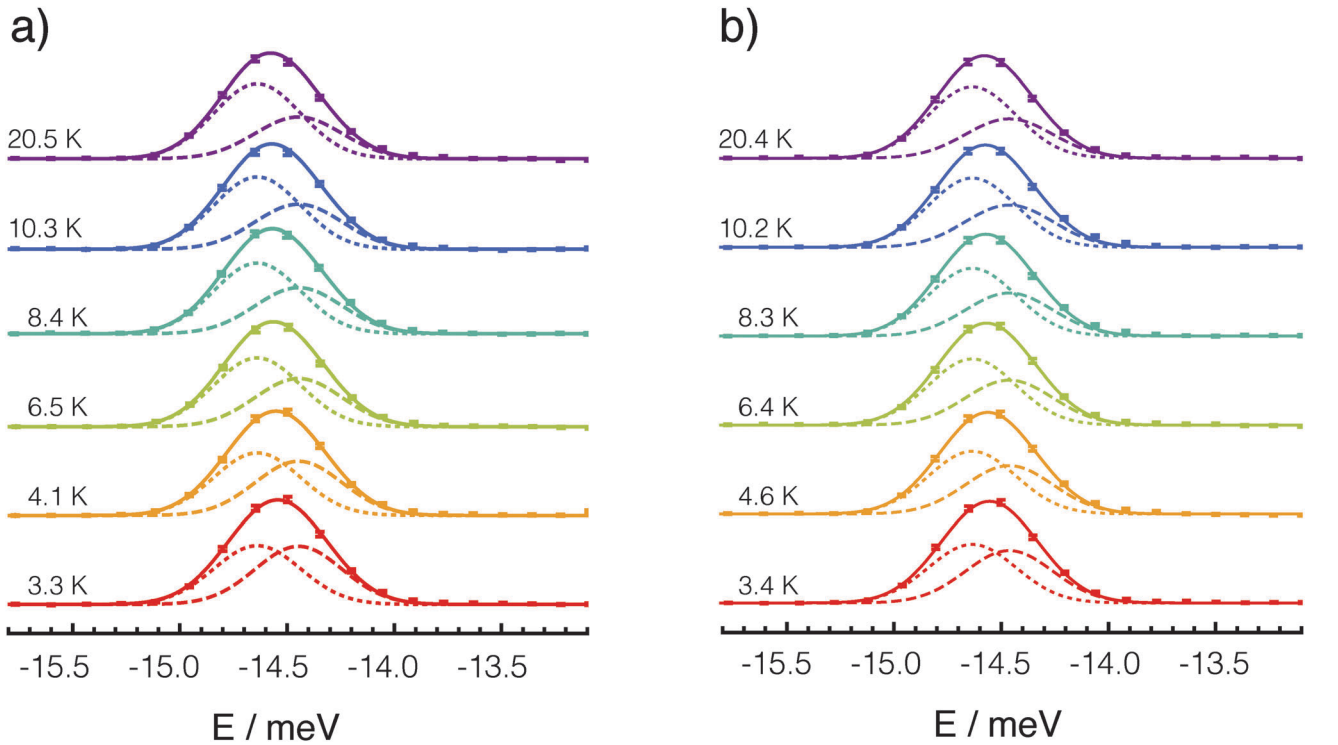

Fig. 3 Inelastic neutron scattering spectra of $H_2@C_{60}$ in energy gain around −14.6 meV in the H-rich phase (a) at 5 kbar applied pressure and (b) at ambient pressure after releasing the pressure at 50 K. Experimental data are represented by points with error bars. The best fit curve with a two Gaussian model is shown as full line for each temperature, while the two components are shown as dashed and dotted lines, respectively.

Table 1 Summary of the best fit values of the energy parameters entering in the two Gaussian model of eqn (1) for the three experimental datasets

	P-rich phase ambient pressure	H-rich phase ambient pressure	H-rich phase 5 kbar
$\bar{E}$/meV	−14.60 ± 0.01	−14.58 ± 0.02	−14.56 ± 0.01
Δ/meV	0.135 ± 0.01	0.17 ± 0.02	0.19 ± 0.02
w/meV	0.45 ± 0.01	0.46 ± 0.02	0.46 ± 0.01

as well as their absolute splitting. Although it is not possible to establish the asymptotic low-temperature trend for the datasets recorded in the pressure cell, the slope of the curves and the temperature at which the curves begin to rise with decreasing temperature, confirm the larger splitting in the H-rich phase as determined by the detailed line-shape fits, either with or without pressure, than in the P-rich phase at no applied pressure.

In all the three sets of experiments the full widths at half maximum are slightly larger than the instrumental resolution allowing us to estimate the inherent line-width of the *ortho* to *para* transitions between 0.3 and 0.4 meV.

4 Quantum dynamics and INS transition probabilities

A good basis for the study of the five-dimensional quantum dynamics of a "rigid" H_2 confined inside a C_{60} cage is given by the product of a translational wave-function $\psi_{NLM}(\mathbf{R})$ with a

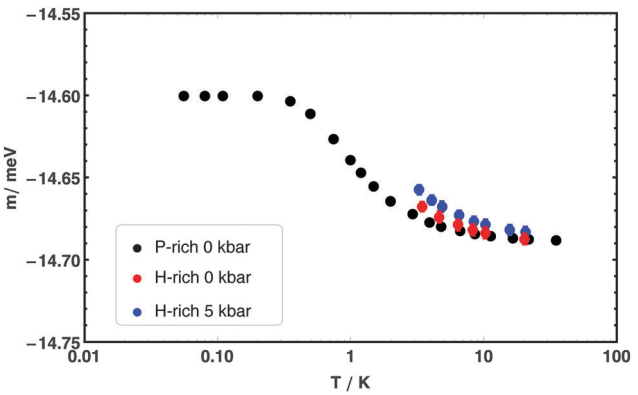

Fig. 4 The temperature dependence of the first moments of the best-fit model, eqn (1), to the INS line for the dataset in the P-rich phase at ambient pressure (black dots), H-rich phase at ambient pressure (red dots) and H-rich phase at 5 kbar (blue dots).

rotational wave-function $Y_{JM_J}(\theta_\mathbf{r},\phi_\mathbf{r})$, where $\mathbf{R} = \{R,\theta_\mathbf{R},\phi_\mathbf{R}\}$ and $\mathbf{r} = \{r,\theta_\mathbf{r},\phi_\mathbf{r}\}$ are the spherical coordinates of centre of mass and the internuclear vector of the H_2 molecule, respectively.[20,21,27] The rotational wave-functions are spherical harmonics Y_{JM_J} identified by the rotational angular momentum J and its projection along a fixed quantisation axis M_J.[41] The translational wave-functions can be decomposed into the product of a radial wave-function $\psi_{NL}(R)$ with a spherical harmonic $Y_{LM_L}(\theta_\mathbf{R},\phi_\mathbf{R})$ where N is the principal (energy) quantum number and L and M_L are the orbital angular momentum quantum

numbers. Within a very good approximation the ground state *ortho* wave-functions are a linear combination of $\psi^o_{00}(R)Y_{00}(\theta_{\mathbf{R}},\phi_{\mathbf{R}})Y_{1m}(\theta_{\mathbf{r}},\phi_{\mathbf{r}})$ with $m = -1, 0, 1$. The ground *para* state wave-function is $\psi^p_{00}(R)Y_{00}(\theta_{\mathbf{R}},\phi_{\mathbf{R}})Y_{00}(\theta_{\mathbf{r}},\phi_{\mathbf{r}})$.[3,4,20,21] At the lowest order in perturbation theory only the rank 2 harmonics of the crystal field potential make a contribution to the quantum dynamics of $J = 1$ *ortho* ground state.[42] Any symmetry breaking potential with the principal axis pointing along the Z laboratory frame is effectively equivalent to:

$$V = \sqrt{20\pi}\delta\left\{ Y_{20}(\theta_{\mathbf{r}},\phi_{\mathbf{r}}) + \frac{\eta}{\sqrt{6}}[Y_{22}(\theta_{\mathbf{r}},\phi_{\mathbf{r}}) + Y_{2-2}(\theta_{\mathbf{r}},\phi_{\mathbf{r}})]\right\} \quad (2)$$

where δ and η represent the anisotropy and the bi-axiality of the potential respectively. In the *ortho* state the solutions of the restricted quantum dynamical problem are

$$\Psi_{1n} = \sum_{m=-1}^{1} \psi^o_0(R)\, Y_{00}(\theta_{\mathbf{R}},\phi_{\mathbf{R}})\, Y_{1m}(\theta_{\mathbf{r}},\phi_{\mathbf{r}})c_{mn} \quad n = -1, 0, 1, \quad (3)$$

where c_{mn} are coefficients of a unitary matrix. The energies are $E_{10} = 2\delta$ and $E_{1\pm1} = -\delta(1 \pm \eta)$.

For a crystal field whose principal axis frame orientation is defined by the Euler angles Ω_{CF}, the eigenstates are obtained by rotation

$$\Psi_{1n}{}' = \sum_{m,m'=-1}^{1} \psi^o_0(R)\, Y_{00}(\theta_{\mathbf{R}},\phi_{\mathbf{R}})\, Y_{1m'}(\theta_{\mathbf{r}},\phi_{\mathbf{r}})D^1_{m'm}(\Omega_{\mathrm{CF}})c_{mn} \quad (4)$$

where $D^1_{mn}(\Omega_{\mathrm{CF}})$ are the coefficients of the rank 1 Wigner matrix[41] rotating the states from the laboratory frame to the crystal field frame. The *para* ground state is a scalar $\Psi_{00}{}' = \Psi_{00}$. Clearly the energy of the levels does not depend on the orientation of the crystal field with respect to the laboratory frame.

As far as intensities are concerned, the number of scattered neutrons is given by

$$N_{\mathrm{tot}}(T) = c\sum_n p_{1n}(T)\bar{W}_{00\leftarrow 1n} \quad (5)$$

where c is a constant depending on the experimental details, $p_{1n}(T)$ is the temperature dependent Boltzmann population of the level $1n$ and $\bar{W}_{00\leftarrow 1n}$ represents the transition probability for a transition between the $1n$ *ortho*-H_2@C_{60} sub-level and the (non-degenerate) 00 *para*-H_2@C_{60} ground state averaged over an isotropic distribution of crystallites. Elaborating the treatment of Yildirim *et al.*[43] the transition probability for the *ortho* to *para* transitions can be written as

$$\begin{aligned} W_{00\leftarrow 1n} &= \frac{k_{\mathrm{f}}}{k_{\mathrm{i}}}\frac{b^2}{4}\left|\left\langle \Psi_{00}{}' \left| e^{i\mathbf{q}\cdot\mathbf{R}} \sin\left(\frac{\mathbf{q}\cdot\mathbf{r}}{2}\right)\right| \Psi_{1n}{}' \right\rangle\right|^2 \\ &= \frac{k_{\mathrm{f}}}{k_{\mathrm{i}}}\frac{b^2}{4}\left[\left\langle \psi^p_{00}(R)\right| j_0(qR)\left|\psi^o_{00}(R)\right\rangle j_1\left(\frac{qr}{2}\right)\right]^2 \\ &\quad \times 4\pi\left|\sum_{m,m'} Y_{1m'}\left(\theta_{\mathbf{q}},\phi_{\mathbf{q}}\right) D^1_{m'm}(\Omega_{\mathrm{CF}})c_{mn}\right|^2 \end{aligned} \quad (6)$$

which depends on the crystallite orientation *via* $D^1_{mn}(\Omega_{\mathrm{CF}})$. Here k_{i} and k_{f} are the modulus of the incident and scattered neutron wave-vector, $\mathbf{q} = \mathbf{k}_{\mathrm{f}} - \mathbf{k}_{\mathrm{i}}$ is the transferred wave-vector, b is the incoherent scattering length of bound ^{1}H and j_0 and j_1 are the order 0 and 1 spherical Bessel functions of first kind.[44] However for an isotropic powder the transition probability simplifies to:

$$\bar{W}_{00\leftarrow 1n} = \frac{k_{\mathrm{f}}}{k_{\mathrm{i}}}\frac{b^2}{4}\left[\left\langle \psi^p_{00}(R)\right| j_0(qR)\left|\psi^o_{00}(R)\right\rangle j_1\left(\frac{qr}{2}\right)\right]^2 \quad (7)$$

after averaging over the crystallites orientations.

The experimental observations are consistent with an axial crystal field ($\eta = 0$) so that there is one singly degenerate level with energy $E_{10} = 2\delta$ and a double degenerate level with energy $E_{1\pm1} = -\delta$. This is in agreement with the expected low temperatures crystal structure of C_{60} as discussed in the introduction. From the experimental splittings, $\delta = -0.045 \pm 0.003$ meV for H_2@C_{60} molecules in the P-rich phase at ambient pressure and δ increases a further 25% and 40% in absolute value in the H-rich phase at no applied pressure and at 5 kbar, respectively. Eqn (7) proves that the transition probability is independent of the state $1n$, justifying the assumptions on which the line-shape analysis is based.

5 Conclusions

The fine structure of the *ortho*-H_2@C_{60} ground state has been studied by probing the INS transition between the $J = 1$ and $J = 0$ state in energy gain on the IN5b TOF spectrometer at the ILL, Grenoble. The experimental observations demonstrated that the three-fold degeneracy of the rotational *ortho*-H_2 ground state is lifted in H_2@C_{60} in the solid phase. It was possible to determine that the three sub-levels with $J = 1$, composing the ground state of *ortho*-H_2@C_{60}, are split into a lower non-degenerate level and a higher double degenerate level shifted 0.135 meV above. The effect of pressure on the fine structure of the $J = 1$ to $J = 0$ line has been investigated as well. Application of pressure affects the size of the splitting of the *ortho* ground state of H_2@C_{60} by modifying the lattice parameter and the orientation of neighbouring molecules. It was observed that the experimental splitting increased by 40% following the application of pressures up to 5 kbar. Although our findings cannot exclude contributions from the reduction in the icosahedral symmetry of the fullerenes, possibly related to the presence of the enclosed hydrogen itself, they conclusively show that the symmetry breaking effects in H_2@C_{60} in are influenced to a large extent by the orientation and proximity of the neighbouring molecules.

Acknowledgements

This work was funded by the UK Engineering and Physical Sciences Research Council (EPSRC) under grant number EP/M001970/1. The authors are indebted to Nicholas J. Turro for providing the original samples and Mark Denning for purifying it.

The authors thank Claude Payre and James Maurice from ILL for their help in setting up the high pressure cell.

References

1 M. H. Levitt, *Philos. Trans. R. Soc., A*, 2013, **371**, 20120429.
2 K. Komatsu, M. Murata and Y. Murata, *Science*, 2005, **307**, 238–240.
3 M. Xu, F. Sebastianelli, Z. Bačić, R. Lawler and N. J. Turro, *J. Chem. Phys.*, 2008, **128**, 011101.
4 M. Xu, F. Sebastianelli, Z. Bačić, R. Lawler and N. J. Turro, *J. Chem. Phys.*, 2008, **129**, 064313.
5 M. Xu, F. Sebastianelli, B. R. Gibbons, Z. Bačić, R. Lawler and N. J. Turro, *J. Chem. Phys.*, 2009, **130**, 1–14.
6 M. Xu and Z. Bačić, *Phys. Rev. B: Condens. Matter Mater. Phys.*, 2011, **84**, 195445.
7 M. Xu, L. Ulivi, M. Celli, D. Colognesi and Z. Bačić, *Phys. Rev. B: Condens. Matter Mater. Phys.*, 2011, **83**, 241403.
8 M. Xu, S. Ye, A. Powers, R. Lawler, N. J. Turro and Z. Bačić, *J. Chem. Phys.*, 2013, **139**, 064309.
9 M. Xu, S. Ye and Z. Bačić, *J. Phys. Chem. Lett.*, 2015, **6**, 3721–3725.
10 B. Poirier, *J. Chem. Phys.*, 2015, **143**, 101104.
11 E. Sartori, M. Ruzzi, N. J. Turro, J. D. Decatur, D. C. Doetschman, R. G. Lawler, A. L. Buchachenko, Y. Murata and K. Komatsu, *J. Am. Chem. Soc.*, 2006, **128**, 14752–14753.
12 M. Carravetta, A. Danquigny, S. Mamone, F. Cuda, O. G. Johannessen, I. Heinmaa, K. Panesar, R. Stern, M. C. Grossel, A. J. Horsewill, A. Samoson, M. Murata, Y. Murata, K. Komatsu and M. H. Levitt, *Phys. Chem. Chem. Phys.*, 2007, **9**, 4879–4894.
13 E. Sartori, M. Ruzzi, R. G. Lawler and N. J. Turro, *J. Am. Chem. Soc.*, 2008, **130**, 12752–12756.
14 N. J. Turro, A. A. Martí, J. Y.-C. Chen, S. Jockusch, R. G. Lawler, M. Ruzzi, E. Sartori, S.-C. Chuang, K. Komatsu and Y. Murata, *J. Am. Chem. Soc.*, 2008, **130**, 10506–10507.
15 J. Y.-C. Chen, A. A. Martí, N. J. Turro, K. Komatsu, Y. Murata and R. G. Lawler, *J. Phys. Chem. B*, 2010, **114**, 14689–14695.
16 N. J. Turro, J. Y.-C. Chen, E. Sartori, M. Ruzzi, A. A. Martí, R. G. Lawler, S. Jockusch, J. López-Gejo, K. Komatsu and Y. Murata, *Acc. Chem. Res.*, 2010, **43**, 335–345.
17 Y. Li, X. Lei, R. G. Lawler, Y. Murata, K. Komatsu and N. J. Turro, *J. Phys. Chem. Lett.*, 2010, **1**, 2135–2138.
18 A. Zoleo, R. G. Lawler, X. Lei, Y. Li, Y. Murata, K. Komatsu, M. Di Valentin, M. Ruzzi and N. J. Turro, *J. Am. Chem. Soc.*, 2012, **134**, 12881–12884.
19 V. Filidou, S. Mamone, S. Simmons, S. D. Karlen, H. L. Anderson, C. W. M. Kay, A. Bagno, F. Rastrelli, Y. Murata, K. Komatsu, X. Lei, Y. Li, N. J. Turro, M. H. Levitt and J. J. L. Morton, *Philos. Trans. R. Soc., A*, 2013, **371**, 20120475.
20 S. Mamone, M. Ge, D. Hüvonen, U. Nagel, A. Danquigny, F. Cuda, M. C. Grossel, Y. Murata, K. Komatsu, M. H. Levitt, T. Rõõm and M. Carravetta, *J. Chem. Phys.*, 2009, **130**, 081103.
21 M. Ge, U. Nagel, D. Hüvonen, T. Rõõm, S. Mamone, M. H. Levitt, M. Carravetta, Y. Murata, K. Komatsu, J. Y.-C. Chen and N. J. Turro, *J. Chem. Phys.*, 2011, **134**, 054507.
22 T. Rõõm, L. Peedu, M. Ge, D. Hüvonen, U. Nagel, S. Ye, M. Xu, Z. Bačić, S. Mamone, M. H. Levitt, M. Carravetta, J. Y.-C. Chen, X. Lei, N. J. Turro, Y. Murata and K. Komatsu, *Philos. Trans. R. Soc., A*, 2013, **371**, 20110631.
23 A. J. Horsewill, S. Rols, M. R. Johnson, Y. Murata, M. Murata, K. Komatsu, M. Carravetta, S. Mamone, M. H. Levitt, J. Y. C. Chen, J. A. Johnson, X. Lei and N. J. Turro, *Phys. Rev. B: Condens. Matter Mater. Phys.*, 2010, **82**, 081410.
24 A. J. Horsewill, K. S. Panesar, S. Rols, J. Ollivier, M. R. Johnson, M. Carravetta, S. Mamone, M. H. Levitt, Y. Murata, K. Komatsu, J. Y.-C. Chen, J. A. Johnson, X. Lei and N. J. Turro, *Phys. Rev. B: Condens. Matter Mater. Phys.*, 2012, **85**, 205440.
25 A. J. Horsewill, K. Goh, S. Rols, J. Ollivier, M. R. Johnson, M. H. Levitt, M. Carravetta, S. Mamone, Y. Murata, J. Y.-C. Chen, J. A. Johnson, X. Lei and N. J. Turro, *Philos. Trans. R. Soc., A*, 2013, **371**, 20110627.
26 M. Xu, M. Jiménez-Ruiz, M. R. Johnson, S. Rols, S. Ye, M. Carravetta, M. S. Denning, X. Lei, Z. Bačić and A. J. Horsewill, *Phys. Rev. Lett.*, 2014, **113**, 123001.
27 S. Mamone, J. Y.-C. Chen, R. Bhattacharyya, M. H. Levitt, R. G. Lawler, A. J. Horsewill, T. Rõõm, Z. Bačić and N. J. Turro, *Coord. Chem. Rev.*, 2011, **255**, 938–948.
28 K. S. K. Goh, M. Jiménez-Ruiz, M. R. Johnson, S. Rols, J. Ollivier, M. S. Denning, S. Mamone, M. H. Levitt, X. Lei, Y. Li, N. J. Turro, Y. Murata and A. J. Horsewill, *Phys. Chem. Chem. Phys.*, 2014, **16**, 21330–21339.
29 Y. Li, X. Lei, S. Jockusch, J. Y.-C. Chen, M. Frunzi, J. A. Johnson, R. G. Lawler, Y. Murata, M. Murata, K. Komatsu and N. J. Turro, *J. Am. Chem. Soc.*, 2010, **132**, 4042–4043.
30 Y. Li, X. Lei, R. G. Lawler, Y. Murata, K. Komatsu and N. J. Turro, *J. Phys. Chem. Lett.*, 2011, **2**, 741–744.
31 Y. Kohama, T. Rachi, J. Jing, Z. Li, J. Tang, R. Kumashiro, S. Izumisawa, H. Kawaji, T. Atake, H. Sawa, Y. Murata, K. Komatsu and K. Tanigaki, *Phys. Rev. Lett.*, 2009, **103**, 073001.
32 M. S. Dresselhaus, G. Dresselhaus and P. C. Eklund, *Science of Fullerenes and Carbon Nanotubes*, Academic Press, 1996.
33 R. Tycko, G. Dabbagh, R. M. Fleming, R. C. Haddon, A. V. Makhija and S. M. Zahurak, *Phys. Rev. Lett.*, 1991, **67**, 1886–1889.
34 P. A. Heiney, *J. Phys. Chem. Solids*, 1992, **53**, 1333–1352.
35 W. I. F. David, R. M. Ibberson, T. J. S. Dennis, J. P. Hare and K. Prassides, *Europhys. Lett.*, 1992, **18**, 219–225.
36 W. I. F. David, R. M. Ibberson, T. J. S. Dennis, J. P. Hare and K. Prassides, *Europhys. Lett.*, 1992, **18**, 735–736.
37 B. Sundqvist, *Adv. Phys.*, 1999, **48**, 1–134.
38 A. J. Horsewill, K. S. Panesar, S. Rols, M. R. Johnson, Y. Murata, K. Komatsu, S. Mamone, A. Danquigny, F. Cuda, S. Maltsev, M. C. Grossel, M. Carravetta and M. H. Levitt, *Phys. Rev. Lett.*, 2009, **102**, 013001.
39 The yellow book, 2008, http://www.ill.eu/instruments-support/instruments-groups/yellowbook.
40 A. J. Horsewill, K. Goh, M. R. Johnson, M. H. Levitt, S. Mamone, J. Ollivier, S. Rols and N. J. Turro, Quantum

dynamics of H2 in the endofullerene H2@C60: Crystal field effects and fine structure in the J = 0 to J = 1 rotational line, 2014, http://doi.ill.fr/10.5291/ILL-DATA.7-05-412.
41 D. A. Varshalovich, A. N. Moskalev and V. K. Khersonskii, *Quantum Theory of Angular Momentum*, World Scientific, Singapore, 1988.
42 F. Reif and E. M. Purcell, *Phys. Rev.*, 1953, **91**, 631–641.
43 T. Yildirim and A. B. Harris, *Phys. Rev. B: Condens. Matter Mater. Phys.*, 2002, **66**, 214301.
44 M. Abramowitz and I. A. Stegun, *Handbook of Mathematical Functions: with Formulas, Graphs, and Mathematical Tables*, Dover Publications, Ninth Dover Printing edn, 1972.